Solar Energy Materials & Solar Cells 120 (2014) 168–174

Contents lists available at ScienceDirect

Solar Energy Materials & Solar Cells

journal homepage: www.elsevier.com/locate/solmat

Efficiency improvement of Si solar cells using metal-enhanced nanophosphor fluorescence

J.-Y. Chen, C.K. Huang, W.B. Hung, K.W. Sun *, T.M. Chen

Department of Applied Chemistry, National Chiao Tung University, Hsinchu 30010, Taiwan

ARTICLE INFO

Article history:
Received 9 April 2013
Received in revised form
12 August 2013
Accepted 27 August 2013
Available online 20 September 2013

Keywords:
Nanophosphor
Luminescence down-shifting
Metal-enhanced fluorescence
Ag nanoparticle

ABSTRACT

In this study, Eu^{2+}-doped barium silicate ($Ba_2SiO_4:Eu^{2+}$) nanophosphors dispersed in a surfactant solution were spin-coated on commercially available silicon solar cells to form colloidal crystals on the surface. The crystals then act as luminescence down-shifting centers to generate low-energy photons for incident ultraviolet light. The fluorescence from the $Ba_2SiO_4:Eu^{2+}$ nanophosphors was further enhanced by coating a metal-enhanced layer composed of Ag nanoparticles and a SiO_2 spacer. The solar cells showed an enhancement of 0.86 mA/cm^2 in short-circuit current density and approximately 0.64% increase in power conversion efficiency when coated with nanophosphors, SiO_2 spacers, and Ag nanoparticles. The properties of cells integrated with the metal-enhanced layer were characterized to identify the roles of nanophosphors and Ag nanoparticles in improved light harvesting. These experiments demonstrated that the colloids of $Ba_2SiO_4:Eu^{2+}$ acted as luminescence down-shifting centers in the ultraviolet region and the metallic nanoparticles also helped to enhance fluorescence in the visible region to increase light absorption within the measured spectral regime.

1. Introduction

The maximum efficiency of a single-junction solar cell is constrained by the Shockley–Queisser limit [1], which defines the maximal output power as a function of the bandgap in a solar cell. Limitations set on the maximum efficiency of the cells are due to the loss mechanisms in solar cells, such as sub-bandgap-energy photon loss [2] and thermalization of charge carriers caused by the absorption of high-energy photons with energies larger than the bandgap of the solar cell. These fundamental losses directly lead to an efficiency limit of approximately 30% for a material with a bandgap of 1.1–1.3 eV under non-concentrated Air Mass 1.5 (AM 1.5) illumination [1].

Various schemes have been proposed to overcome this fundamental efficiency limit for single-junction solar cells [3–5]. However, these steps are either difficult to implement or expensive to mass produce. One way to surpass this limit is using a luminescence down-shifting (LDS) process to absorb high-energy photons and re-emit them at longer wavelengths such that the photovoltaic device exhibits a significantly better response. The application of an LDS layer was first demonstrated in the late 1970s to improve the poor spectral response of solar cells to short-wavelength light. The LDS layer can help harvest full solar energy by expanding the operating spectral range toward the ultraviolet (UV) range. A recent theory demonstrated that a conversion efficiency of 38.6% can be achieved under unconcentrated sunlight using a silicon solar cell with an ideal LDS material [6]. Detailed reviews of the progress in this area can be found in Refs. [7–14].

An increase of 0.3% (absolute) was reported when an organic luminescent dye is included in the ethylene vinyl acetate (EVA) encapsulation layer of multicrystalline silicon photovoltaic modules [15]. Thermodynamic evaluation and analysis involving both lossless and lossy theoretical limits have further demonstrated that 7% efficiency improvement in efficiency can be achieved using a perfectly down-converting material [16]. The down-conversion process increases the short-circuit current while retaining the open-circuit voltage. For semiconductor nanoparticles, the high surface-to-volume ratio may possibly create a high concentration of mid-level trap states and coalesce into a band that function in doubly radiative emission processes in an efficiency manner [5,16,17]. Therefore, the increase in surface traps could be advantageous for the LDS process for the nanophosphors as well. Furthermore, if nanoparticles are embedded within the top layer of the solar cells, then the scattering becomes inconsequential and the inherent scattering property in a down-converting layer could be solved. This becomes an advantage for any three-dimensional configuration of the down-conversion layer [16]. For example, YVO_4 nanophosphors were directly integrated into the textured solar cell surface without host materials. The proposed hybrid system showed a 4% enhancement in short-circuit current density

* Corresponding author. Tel.: +886 3 5712121.
E-mail address: kwsun@mail.nctu.edu.tw (K.W. Sun).

0927-0248/$ - see front matter © 2013 Elsevier B.V. All rights reserved.
http://dx.doi.org/10.1016/j.solmat.2013.08.039

and approximately 0.7% in power conversion efficiency using AM 1.5 illumination [18].

At the other end of the spectrum, interactions of metallic surface or particles are attracting increased interest. Near-field interactions are those occurring within a wavelength distance of an excited phosphors/fluorophores [19,20]. The spectral properties of fluorescence materials can be altered by near-field interactions with the electron plasma present in metals by several methods that have not been used in classical fluorescence experiments. Experimental results showing the effects of fluorophore-to-silver distance on the emission of cyanine-dye-labeled oligonucleotides suggest that silver island films yield improved fluorescence measurements and maximum fluorescence enhancements occur at approximately 9 nm from the metal surface [21]. The effects of metals on fluorescence are explained using a concept based on radiating plasmons [22]. Wavenumber matching considerations can be used to predict whether fluorophores at a given distance from a continuous planar are emitted or quenched. A twofold enhancement in structured fluorescence is also observed in perylene in close proximity to silver island films [23]. The emission of cerium-doped yttrium aluminum garnet (YAG:Ce) phosphor thin films can be enhanced by surface plasmon coupling to a suitably nanostructured silver-island layer. The photoluminescence intensity is significantly enhanced by capping Ag islands with a 10 nm-thick SiO_2 layer as a dielectric medium [24].

The current study demonstrates the increase in conversion efficiency of Si solar cells by combining rare-earth element-doped barium silicate ($Ba_2SiO_4:Eu^{2+}$) nanophosphors, Ag NPs, and SiO_2 dielectric spacer directly onto the textured surface of the devices. $Ba_2SiO_4:Eu^{2+}$ is a widely used optical material with many good features, including excellent thermal efficiency and high luminescent quantum efficiency [25,26]. UV or visible excitation for $Ba_2SiO_4:Eu^{2+}$ nanophosphors produces broadband luminescence with peak wavelengths of 505 nm. Therefore, $Ba_2SiO_4:Eu^{2+}$ phosphors are promising UV-absorbing spectral converters for solar cells because they possess broadband absorption throughout the entire UV region (300–450 nm) and they enable the emission of intense visible lights. Thus, these materials are well suited for spectral conversion in solar cells. The current study aims to investigate the quantum efficiency enhancement associated with metal-enhanced light harvesting and energy transfer properties of $Ba_2SiO_4:Eu^{2+}$ nanophosphors.

2. Experimental

Fig. 1 shows a schematic diagram of the synthesis of a micro-textured cell surface covered with nanophosphors, SiO_2 dielectric layer, and Ag NPs ($Ba_2SiO_4:Eu^{2+}/SiO_2$/Ag NPs). The crystalline Si (c-Si) solar cell device used was manufactured following the procedures reported in Ref. [27]. Given that incident UV radiations mostly produce electron–hole pairs near the device surface, photo-generated carriers easily disappear by recombining with surface defects, which can lead to inferior cell efficiency. However, in the presence of the Ba_2SiO_4 nanophosphors on the front side, more photons can be absorbed closer to the depletion region when the UV photons are luminescence down-shifted to the visible region. The built-in electric field automatically separates the photo-generated electron–hole pairs and enhances the photovoltaic effect.

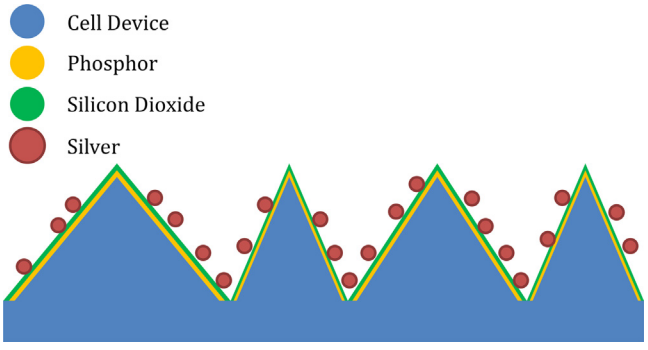

Fig. 1. Schematic of textured cell structures covered with Ba_2SiO_4:7% Eu^{2+} nanophosphors, SiO_2 layer, and Ag NPs.

Barium nitrate ($Ba(NO_3)_2$), europium nitrate pentahydrate ($Eu(NO_3)_3 \cdot 5H_2O$), tetraethyl orthosilicate (TEOS), and ethylene glycol (EG) were purchased from Sigma-Aldrich. Citric acid (CA) and 28% ammonium hydroxide (NH_4OH) were supplied by Showa (Chemical Co., Ltd., Tokyo, Japan). Ag NPs dissolved in deionized water at a concentration of 100 ppm and average diameters of 10–20 nm were purchased from Particular GmbH. All reagents were used as received.

$(Ba_{1-x}Eu_x)_2SiO_4$ ($0 \le x \le 0.09$) compounds were synthesized by the typical Pechini method. Stoichiometric amounts of $Ba(NO_3)_2$, $Eu(NO_3)_3 \cdot 5H_2O$, and CA were dissolved in deionized water. Subsequently, TEOS mixed in ethanol and EG were added to the mixture solution under vigorous stirring, and the pH was adjusted to 2 with NH_4OH. The molar ratio of CA to cations and to EG was 4:1:2. The solution was heated on a hot plate at 80 °C for 3 h to yield a transparent solution, and then the temperature was increased to 150 °C for water evaporation. When the solution turned into a viscous brown gel, it was dried at 100 °C in air overnight. A fine precursor powder was produced by calcining the dry gel in air at various temperatures (250–500 °C) for a few hours. After eliminating organic content, the porous powder was ground and annealed at 900 °C for 6 h in reducing atmosphere (5% H_2+95% N_2). Then, Ba_2SiO_4:7% Eu^{2+} phosphor with pale-green appearance was obtained.

To determine the optimum SiO_2 film thicknesses and nanophosphor concentration for maximizing the fluorescence intensity in the visible region, the $Ba_2SiO_4:Eu^{2+}/SiO_2$/Ag NPs layers were first fabricated on a planar Si surface. The Ba_2SiO_4 nanophosphors were dispersed in ethanol to obtain a 1, 2, and 3 mg/ml solutions, respectively. Spin-coating was used for nanophosphor deposition. Using 1, 2, and 3 mg/ml of the Ba_2SiO_4 nanophosphors, uniform and perfect-light-scattering thin films with a thickness of approximately 100 nm were obtained under properly controlled spin-coating rates. Six samples with SiO_2 spacer thicknesses ranging from 5 nm to 100 nm were deposited onto the nanophosphor layer using a plasma-enhanced chemical vapor deposition (PECVD) system followed by spin-coating of the Ag NPs. The decay times of the metal-enhanced and down-shifted photoluminescence were measured using a time-correlated single photon counting (TCSPC) system with spectral resolution and system response of 0.1 meV and 300 ps, respectively. To determine the optimal particle density of the nanophosphors, electrical characterizations on solar cells coated with nanophosphors of different densities were performed by varying the concentrations of the nanophosphors solution from 1 mg/ml to 3 mg/ml.

After optimal parameters were determined, the integrated $Ba_2SiO_4:Eu^{2+}/SiO_2$/Ag NPs layers were fabricated on textured c-Si solar cells. The c-Si cells with and without $Ba_2SiO_4:Eu^{2+}/SiO_2$/Ag NPs layers were evaluated at room temperature based on the illuminated current density versus voltage (J–V) characteristics, external quantum efficiency (EQE), and reflectance. Photocurrent was analyzed using a solar simulator under the Air Mass 1.5 Global (AM 1.5G) illumination condition (100 mW/cm^2, 25 °C). The EQE was measured using an AM 1.5G standard spectrum and an Optosolar simulator (SR-150). The reflectance spectra of the samples were recorded using a UV–vis–NIR spectrophotometer

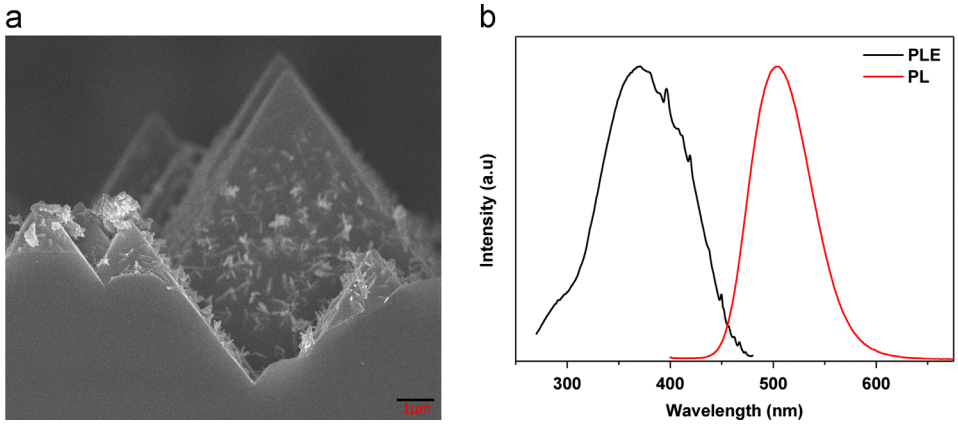

Fig. 2. (a) SEM image of the Ba_2SiO_4:7% Eu^{2+} and (b) PLE (black curve) and PL (red curve) spectra of Ba_2SiO_4 nanophosphors in ethanol. (For interpretation of the references to color in this figure legend, the reader is referred to the web version of this article.)

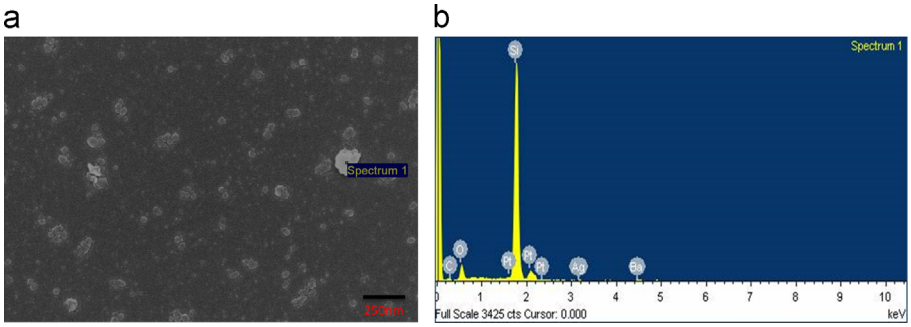

Fig. 3. (a) Low-magnification SEM image of Ba_2SiO_4 nanophosphor colloids deposited directly on the planar Si surface and (b) EDS spectrum of Ba_2SiO_4 nanophosphors.

(Hitachi U-4100) at wavelengths ranging from 200 nm to 1200 nm. X-ray diffraction (XRD) of the samples was measured using a Bruker AXS D8 advanced automatic diffractometer with Cu Kα radiation. The PL spectra of the nanophosphors were measured using a Spex Fluorolog-3 Spectrofluorometer equipped with a 450 W Xe light source. The quantum efficiency (QE) of the nanophosphors was measured using an integrating sphere, whose inner face was coated with Spectralon equipped with a spectrofluorometer (Horiba Jobin-Yvon Fluorolog 3-22 Tau-3). The corresponding optical absorbance (φ) and quantum efficiency (η) were calculated using the equations from Ref. [28].

3. Results and discussion

Fig. 2 (a) shows the scanning electron microscopy (SEM) image of the Ba_2SiO_4:7% Eu^{2+} nanophosphors. The nanophosphors had a needle-like shape with an average diameter of ~40 to 50 nm and a length of approximately 140 nm. The size distribution of the nanophosphors was further confirmed by dynamic light scattering (DLS) measurements. Fig. 2(b) shows the photoluminescence excitation (PLE) and fluorescence spectra of the Ba_2SiO_4 nanophosphors in ethanol. The fluorescence spectrum showed a major emission at 505 nm when the particles were excited at a wavelength of 350 nm. The PLE spectrum was measured at a fixed detection wavelength of 505 nm. The spectrum showed a broad resonance expansion from 300 nm to 450 nm with a peak centered at around 360 nm, indicating that the Ba_2SiO_4 nanophosphors exhibited the photon down-shifting by absorbing UV photons and converting them into visible light with a high luminescent QE of approximately 40%.

The low-magnification SEM image in Fig. 3(a) shows the as-prepared Ba_2SiO_4/SiO_2/Ag NPs layers on the planar Si surface at a concentration of 2 mg/ml. The presence and compositions of the nanophosphors were confirmed by energy-dispersive spectroscopy (EDS) results (Fig. 3(b)). The thickness of the as-deposited SiO_2 spacer layers was verified by the EDS mapping technique. For example, Fig. 4(a) and (b) shows the EDS mapping results of a sample deposited with a 100 nm-thick SiO_2 layer. The aforementioned Ag NPs dispersed in deionized water were then spin-coated onto the SiO_2 dielectric layers. The EDS spectrum and SEM image of the very dilute Ag NP coated on the texture surface of the c-Si solar cells are shown in Fig. 5. The estimated Ag NP density was far below 4×10^7 cm^{-2}. The Ag NPs were also found to form small aggregates on the texture. Fig. 6 shows the down-shifted PL spectra excited at 396 nm of nanophosphors separated from the Ag NPs as a function of dielectric layer thicknesses. The PL intensity as a function of oxide thickness only is also shown in the inset of Fig. 6. The spectrum of the nanophosphors without the metal-enhanced layer is also displayed for comparison. The enhancement in PL intensity strongly depended on the SiO_2 layer thickness and reached the maximum at a thickness value of 15 nm. The intensity considerably decreased with increased layer thickness of SiO_2 above 60 nm. Base on the PL results (inset of Fig. 6), the plasma ion bombardment during the growth of the SiO_2 layer has a minimum effect on the quality of phosphor layer. The time-resolved spectra for the samples were obtained, and the PL decay times were determined by the methods provided in Ref. [24,29]. The decay times were plotted as a function of SiO_2 layer thicknesses in Fig. 7. At the maximum PL enhancement, we extracted a decay time of 612.6 ns, which was much shorter than the case without the metal-enhanced layer. This result indicated that nearby Ag NPs can increase the intrinsic radiative decay rate of

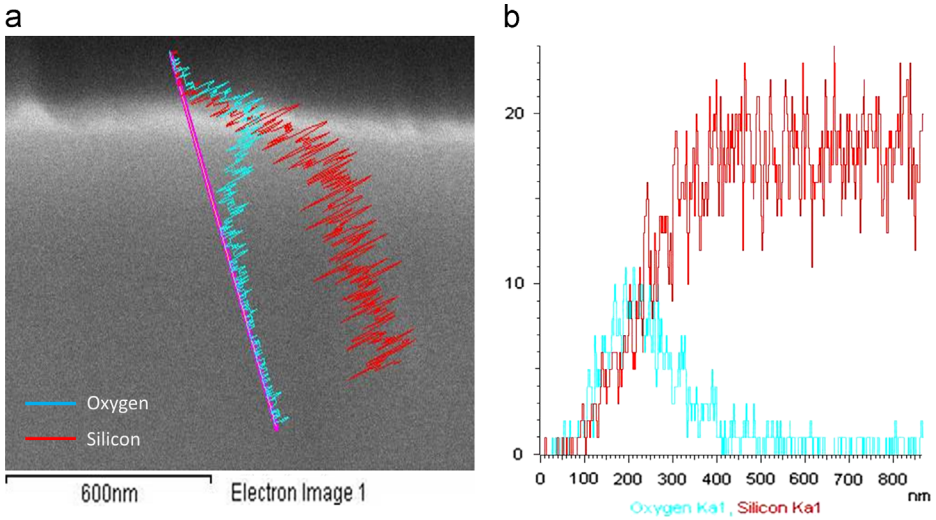

Fig. 4. (a) Cross-section SEM image of the SiO_2 spacer. (b) EDS mapping results of the 100 nm thick SiO_2 layer in (a). Distribution profiles of oxygen and silicon are plotted in blue and red, respectively. (For interpretation of the references to color in this figure legend, the reader is referred to the web version of this article.)

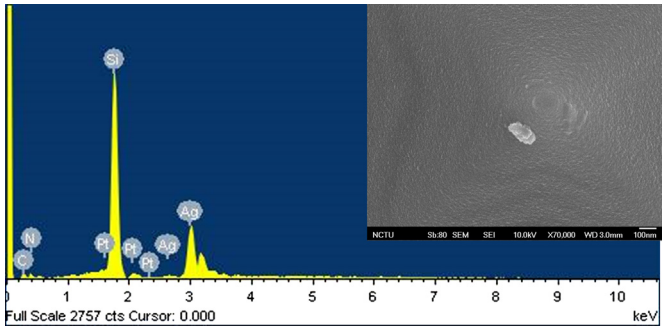

Fig. 5. SEM image and EDS results of dilute Ag NPs on texture c-Si surface.

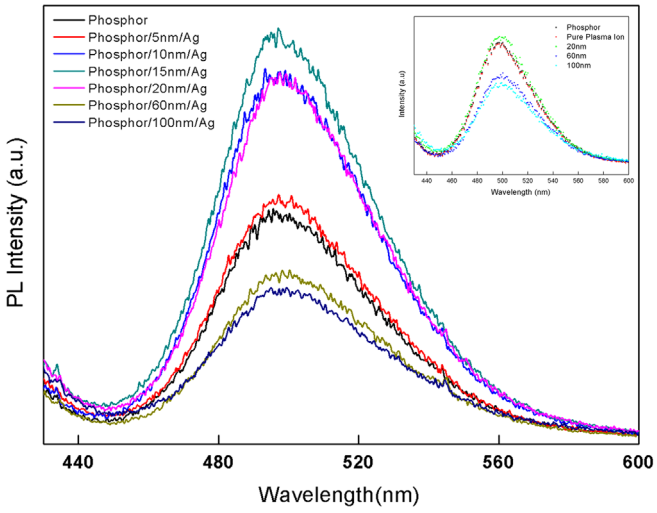

Fig. 6. Down-shifted PL spectra excited at 396 nm from nanophosphors separated from the Ag particles as a function of SiO_2 spacer thicknesses. The inset shows the PL intensity as a function of oxide thickness only and after the ion bombardment in the PECVD process.

the nanophosphors, i.e., to modify the rate at which a nanophosphor emits photons. Our results suggested that the maximum fluorescence enhancement occurred at around 15 nm from the Ag NPs, in good agreement with earlier reports [21,24].

Electrical characterizations of solar cells coated only with Ba_2SiO_4 nanophosphors with varying concentrations of nanophosphors

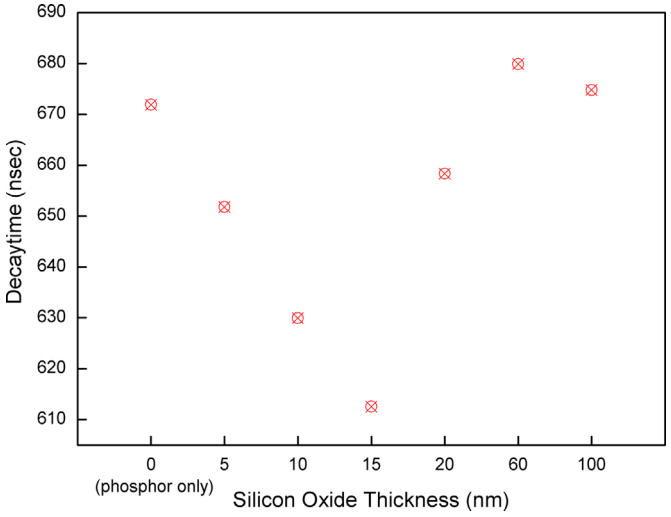

Fig. 7. Decay times of down-shifted PL from nanophosphors as a function of SiO_2 layer thicknesses. Decay time of the sample coated with nanophosphor only is also displayed for comparison.

solution from 1 mg/ml to 3 mg/ml are shown in Fig. 8. These results were used to determine the optimal nanophosphor density for a better power conversion efficiency. Fig. 9 displays the high-magnification SEM cross-section images of the Ba_2SiO_4 nanophosphor coated on the texture Si solar cell surface. The highest efficiency increase (~0.2%) was achieved when the solar cell surface was covered with nanophosphors at 2 mg/ml. The cell efficiency deteriorated when the particle densities were higher than 3 mg/ml. This phenomenon was attributed to the substantial absorption in the UV region by nanophosphors, which led to the considerable loss of the original UV transmittance toward the cell. Fig. 10 shows the *J–V* characteristics of the solar cell at the maximum enhancement. The performance of the cell without nanophosphors was also presented for comparison. V_{oc} and FF remained almost unaffected with increased J_{sc} from 41.18 mA/cm^2 to 41.51 mA/cm^2 with the integrated nanophosphors. Therefore, the enhancement in cell efficiency can indeed be attributed to the increase in photocurrent and light absorption.

Subsequently, a series of solar cell samples was prepared and characterized at different preparation stages based on the structures in Fig. 1 using an optimal concentration of 2 mg/ml Ba_2SiO_4 nanophosphor solution and SiO_2 layer thicknesses of 10, 15, and

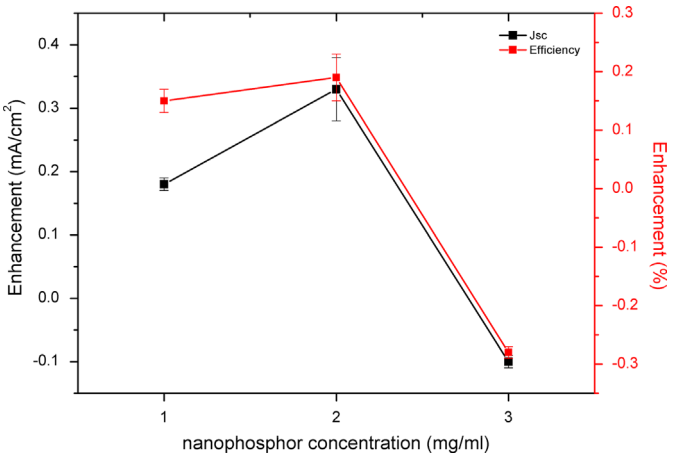

Fig. 8. Enhancement in power conversion efficiency and short-circuit current as a function of nanophosphor concentrations.

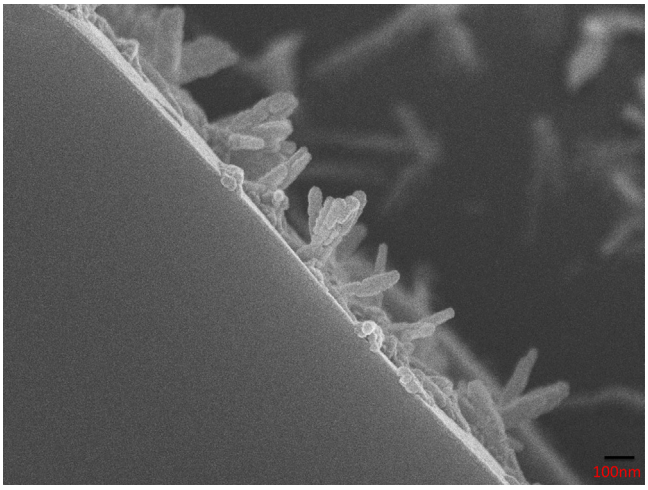

Fig. 9. Cross-section SEM images at high magnification of the Ba_2SiO_4 nanophosphors coated on the texture Si solar cell surface at 3 mg/ml.

20 nm. The electrical characterizations of these solar cells are summarized in Fig. 11. The conversion efficiencies slightly increased when the cells were coated with nanophosphors only. The efficiency increased by nearly 0.7% when the solar cell surface was covered with Ag NPs and a 20 nm SiO_2 spacer.

Fig. 12 shows the changes in the reflectance of the solar cells at maximum performance. The spectra of the bare solar cells and cells with nanophosphor only are also displayed for comparison. The most significant change in the reflectance was observed in the spectral region around 320 nm, which may be ascribed to the absorption by Ba_2SiO_4 nanoparticles. However, at the optimal nanoparticle density of 2 mg/ml, the reflectance in the UV only decreased by $<4\%$ compared that in the cell without nanophosphors and metal-enhanced layer. This result indicated that the EQE of the original cell in the UV was unaffected by the presence of the metal-enhanced layer.

EQE measurements were performed to understand the mechanisms underlying the enhanced cell efficiency. The EQE of the c-Si solar cells prepared at maximum performance was measured relative to the bare cells without nanophosphors and metal-enhanced structures (Fig. 13). The observed EQE enhancement between 500 nm and 600 nm is possibly due to increased lateral light scattering by the Ag nanoparticles, which tends to guide the light into directions that are then totally internally reflected. The presence of the nanophosphors clearly increased

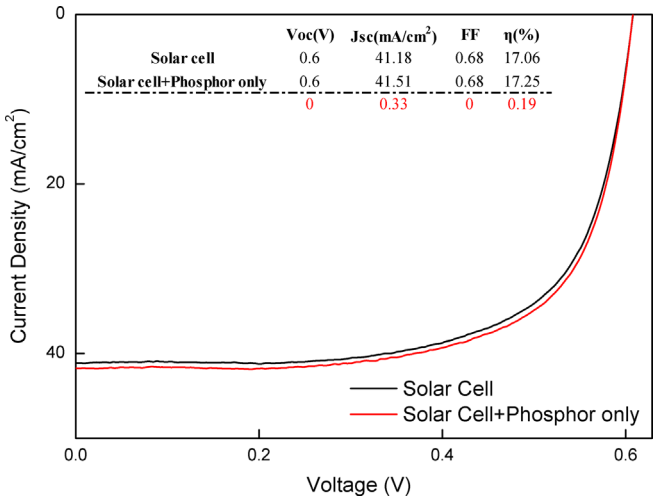

Fig. 10. *J–V* characteristics of the solar cell coated with nanophosphors only at the optimal areal nanophosphor density.

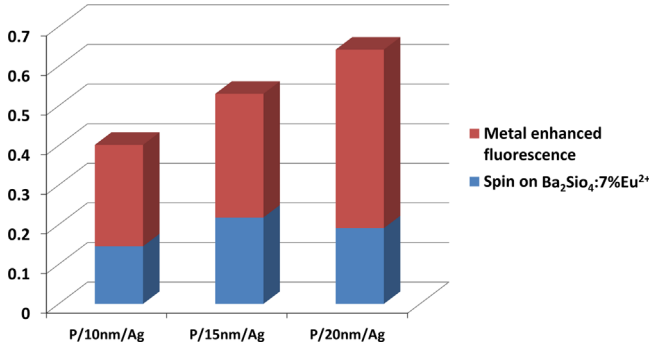

Fig. 11. Efficiency enhancement of solar cells with nanophosphor only and with nanophosphors + metal-enhanced layer as a function of spacer thickness.

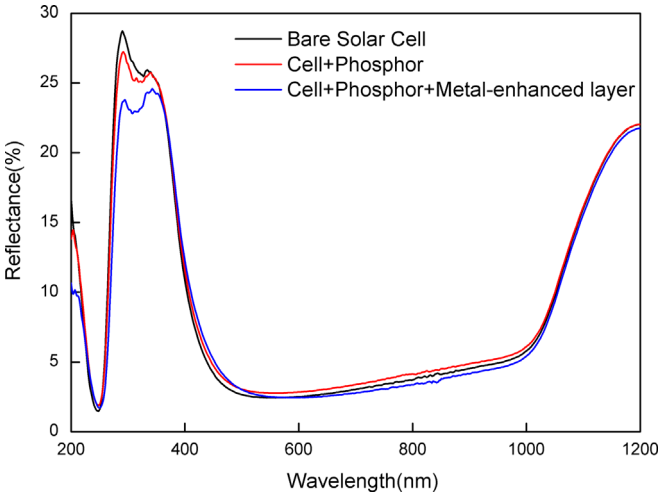

Fig. 12. Reflectance spectra of the solar cells prepared at different stages.

EQE in the UV, indicating that the increase in photocurrent was mostly due to the enhanced absorption of UV by nanophosphors. The EQE measurements agreed with the reflectance results, indicating that the cell response improved in the UV wavelength ranges because of the combined effects from LDS and PL enhancement by Ag NPs.

Fig. 14 shows the *J–V* characteristics of the solar cell at maximum enhancement. The performance of the bare cell is also presented for comparison. The results showed that V_{oc} and FF

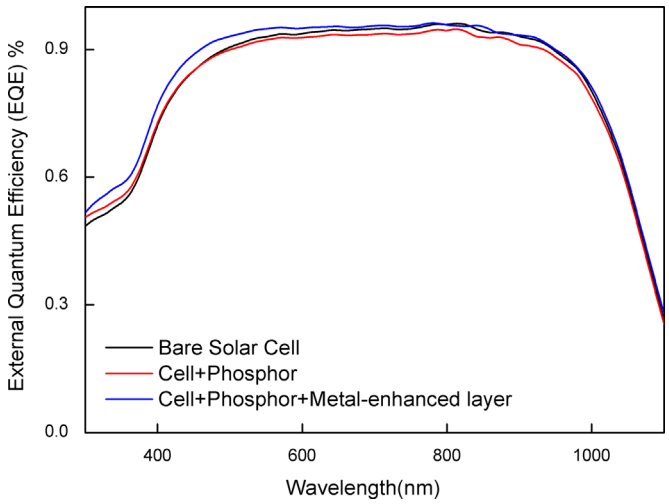

Fig. 13. EQE spectra of the solar cells prepared at different stages.

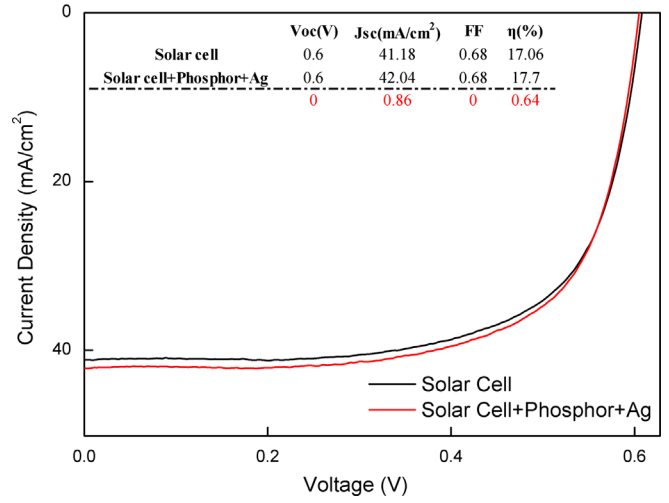

Fig. 14. *J–V* characteristics of the optimized solar cells integrated with 2 mg/ml of the nanophosphors and a spacer thickness of 15 nm. Result from a device without nanophosphor and metal-enhanced layer treatment is displayed for comparison.

remained almost unaffected with increased J_{sc} from 41.18 mA/cm^2 to 42.04 mA/cm^2 with the integrated Ba_2SiO_4 nanophosphors and metal-enhanced layer. Therefore, the enhancement in cell efficiency can indeed be attributed to the increase in photocurrent and light absorption. This finding agreed with the improved EQE (Fig. 13).

Ba_2SiO_4 nanophosphors are LDS materials with a wide UV absorption band and a high luminescent quantum efficiency (~40%). Thus, these nanophosphors can be used to achieve enhanced solar cell performance because they are of low cost, easy to manufacture, and environmental friendly. The Ba_2SiO_4 nanophosphors also do not undergo oxidation and thus have higher stability for efficiency enhancement over solar cells coated with semiconductor quantum dots (QDs)/NPs, such as Si QDs. In addition to the novel property of LDS shown in the current report, the surface roughness of the cells increased after the deposition of the Ba_2SiO_4 nanophosphors, which could possibly reduce the sensitivity of the devices at incident light angles. Thus, we speculated that the photons that reached the Ba_2SiO_4–air interface had more chances of being trapped in the solar cell and were then converted to photocurrents, especially at dawn and sunset (large incident angles).

4. Conclusion

In summary, Ba_2SiO_4 nanophosphors and a metal-enhanced layer were directly integrated into the textured Si solar cell surface. The proposed hybrid system enhanced the power conversion efficiency using AM 1.5 illumination. The observed enhancement can be attributed to LDS and metal-enhanced emission. Unprecedented device performance can be expected with further improvement in LDS quantum yield and fluorescence bandwidth in the visible region. This approach may have promising applications in other types of solar cells and opens new possible schemes for utilizing nanophosphors and metal NP enhancement in energy devices.

Acknowledgments

This work was partially supported by the Bureau of Energy in Taiwan, National Science Council of the Republic of China (Contract no. NSC 101-2917-I-009-005, 99-2119-M-009-004-MY3, and 101-2918-I-009-002) and the Approaching Top University (ATU) Program of the Ministry of Education of the Republic of China.

References

[1] W. Shockley, H.J. Queisser, Detailed balance limit of efficiency of p–n junction solar cells, Journal of Applied Physics 32 (1961) 510–519.
[2] Goldschmidt J.C., Fischer S., Löper P., Krämer K.W., Biner D., Hermle M., et al. Upconversion to enhance silicon solar cell efficiency—detailed experimental analysis with both coherent monochromatic irradiation and white light illumination. In: Proceedings of the 25th european photovoltaic solar energy conference and Exhibition (25th EU PVSEC) Goldschmidtyr, (2010) 229–233.
[3] S.M. Bedair, M.F. Lamorte, J.R. Hauser, A two-junction cascade solar-cell structure, Applied Physics Letters 34 (1979) 38–39.
[4] M. Taguchi, K. Kawamoto, S. Tsuge, T. Baba, H. Sakata, M. Morizane, et al., HIT (TM) cells—high-efficiency crystalline Si cells with novel structure, Progress in Photovoltaics 8 (2000) 503–513.
[5] A. Luque, A. Martí, Increasing the efficiency of ideal solar cells by photon induced transitions at intermediate levels, Physical Review Letters 78 (1997) 5014–5017.
[6] T. Trupke, M.A. Green, P. Wurfel, Improving solar cell efficiencies by down-conversion of high-energy photons, Journal of Applied Physics 92 (2002) 1668–1674.
[7] E. Klampaftis, D. Ross, K.R. McIntosh, B.S. Richards, Enhancing the performance of solar cells via luminescent down-shifting of the incident spectrum: a review, Solar Energy Materials and Solar Cells 93 (2009) 1182–1194.
[8] B.S. Richards, Luminescent layers for enhanced silicon solar cell performance: down-conversion, Solar Energy Materials and Solar Cells 90 (2006) 1189–1207.
[9] V. Badescu, A.D. Vos, Influence of some design parameters on the efficiency of solar cells with down-conversion and down shifting of high-energy photons, Journal of Applied Physics 102 (2007) 073102 (7 pp.).
[10] V. Badescu, A.D. Vos, A.M. Badescu, A. Szymanska, Improved model for solar cells with down-conversion and down-shifting of high-energy photons, Journal of Physics D: Applied Physics 40 (2007) 341–352.
[11] W.G.J.H.M. van Sark, Simulating performance of solar cells with spectral downshifting layers, Thin Solid Films 516 (2008) 6808–6812.
[12] W.G.J.H.M. van Sark, A. Meijerink, R.E.I. Schropp, J.A.M. van Roosmalen, E.H. Lysen, Enhancing solar cell efficiency by using spectral converters, Solar Energy Materials and Solar Cells 87 (2005) 395–409.
[13] T. Maruyama, J. Bandai, Solar cell module coated with fluorescenct coloring agent, Journal of the Electrochemical Society 146 (1999) 4406–4409.
[14] T. Maruyama, R. Kitamura, Transformations of the wavelength of the light incident upon CdS/CdTe solar cells, Solar Energy Materials and Solar Cells 69 (2001) 61–68.
[15] E. Klampaftis, M. Congiu, N. Robertson, B.S. Richards, Luminescent ethylene vinyl acetate encapsulation layers for enhancing the short wavelength spectral response and efficiency of silicon photovoltaic modules, IEEE Journal of Photovoltaics 1 (2011) 29–36.
[16] Z.e.R. Abrams, A. Niv, X. Zhang, Solar energy enhancement using down-converting particles: a rigorous approach, Journal of Applied Physics 109 (2011) 114905 (9 pp.).
[17] A. Luque, A. Martí, E. Antolín, C. Tablero, Intermediate bands versus levels in non-radiative recombination, Physica B 382 (2006) 320–327.
[18] C.K. Huang, Y.C. Chen, W.B. Hung, T.M. Chen, K.W. Sun, W.L. Chang, Enhanced light harvesting of Si solar cells via luminescent down-shifting using YVO_4: $Bi3^+$, $Eu3^+$ nanophosphors, Progress in Photovoltaics: Research and Applications (2012), http://dx.doi.org/10.1002/pip.2222.

[19] C.D. Geddes, J.R. Lakowicz, Metal-enhanced fluorescence, Journal of Fluorescence 12 (2002) 121–129.
[20] Joseph R. Lakowicz, Krishanu Ray, Mustafa Chowdhury, Henryk Szmacinski, Yi Fu, Jian Zhang, et al., Plasmon-controlled fluorescence: a new paradigm in fluorescence spcetroscopy, Analyst 133 (2008) 1308–1346.
[21] J. Malicka, I. Gryczynski, Z. Gryczynski, J.R. Lakowicz, Effects of fluorophore-to-silver distance on the emission of cyanine-dye-labeled oligonucleotides, Analytical Biochemistry 315 (2003) 57–66.
[22] R. Joseph, Lakowicz, Radiative decay engineering 5: metal-enhanced fluorescence and plasmon emission, Analytical Biochemistry 337 (2005) 171–194.
[23] Y.X. Zhang, K. Aslan, M.J.R. Previte, C.D. Geddes, Metal-enhanced fluorescence: Surface plasmons can radiate a fluorophore's structured emission, Applied Physics Letters 90 (2007) 053107 (3 pp.).
[24] Wen-Hsuan Chao, Ren-Jye Wu, Chih-Song Tsai, Tai-Bor Wu, Surface plasmon-enhanced emission from Ag-coated Ce doped $Y_3Al_5O_{12}$ thin films phosphor capped with a dielectric layer of SiO_2, Journal of Applied Physics 107 (2010) 013101–013105.
[25] Y. Eagleman, E. Bourret-Courchesne, S.E. Derenzo, Investigation of Eu^{2+} doped barium silicates as scintillators, IEEE Transactions on Nuclear Science 59 (2012) 479–486.
[26] M. Yamaga, Y. Masui, S. Sakuta, N. Kodama, K. Kaminaga, Radiative and nonradiative decay processes responsible for long-lasting phosphorescence of Eu^{2+}-doped barium silicates, Physical Review B 71 (2005) 205102 (7 pp.).
[27] C.K. Huang, H.H. Lin, J.Y. Chen, K.W. Sun, W.L. Chang, Efficiency enhancement of the poly-silicon solar cell using self-assembled dielectric nanoparticles, Solar Energy Materials and Solar Cells 95 (2011) 2540–2544.
[28] J.C. deMello, H.F. Wittmann, R.H. Friend, An improved experimental determination of external photoluminescence quantum efficiency, Advanced Materials 9 (1997) 230–232.
[29] L. Wang, T. Li, Y. Du, C.G. Chen, L. Li, M. Zhou, et al., Au NPs-enhanced surface plasmon resonance for sensitive detection of mercury(II) ions, Biosensors and Bioelectronics 25 (2010) 2622–2626.